Research Article | Vol. 26, No. 14 | 9 Jul 2018 | OPTICS EXPRESS 18320
Optics EXPRESS

Highly transmissive subtractive color filters based on an all-dielectric metasurface incorporating TiO_2 nanopillars

ISHWOR KOIRALA,[1] SANG-SHIN LEE,[1,4] AND DUK-YONG CHOI[2,3,5]

[1]*Department of Electronic Engineering, Kwangwoon University, 20 Kwangwoon-ro, Nowon-gu, Seoul 01897, South Korea*
[2]*Laser Physics Centre, Research School of Physics and Engineering, Australian National University, Canberra, ACT 2601, Australia*
[3]*College of Information Science and Technology, Jinan University, Guangzhou, Guangdong, 510632, China*
[4]*slee@kw.ac.kr*
[5]*duk.choi@anu.edu.au*

Abstract: Transmissive subtractive color filters are proposed and demonstrated that take advantage of an all-dielectric metasurface based on a lattice of TiO_2 nanopillars (NPs), rendering a high transmission efficiency that exceeds 90%. TiO_2 NP elements have been created that exhibit a high aspect ratio. Specifically, a series of lithographic processes are conducted to form a narrow and deep hole in the photoresist, which is accompanied by atomic layer deposition of TiO_2. A broad palette of vivid colors encompassing the visible band has been obtained by adjusting the NP diameter for a constant duty ratio of 0.35. For the NP resonator, the electric and magnetic field profiles in conjunction with the scattering cross-sections have been meticulously investigated to theoretically validate that the resonant transmission dips are primarily governed by the simultaneous excitation of an electric dipole and a magnetic dipole via Mie scattering.

OCIS codes: (230.7408) Wavelength filtering devices; (350.4238) Nanophotonics and photonic crystals; (290.4020) Mie theory; (160.4670) Optical materials; (330.1710) Color, measurement; (140.4780) Optical resonators.

References and links

1. S. Kinoshita and S. Yoshioka, "Structural colors in nature: the role of regularity and irregularity in the structure," ChemPhysChem **6**(8), 1442–1459 (2005).
2. K. Kumar, H. Duan, R. S. Hegde, S. C. Koh, J. N. Wei, and J. K. Yang, "Printing colour at the optical diffraction limit," Nat. Nanotechnol. **7**(9), 557–561 (2012).
3. H. J. Park, T. Xu, J. Y. Lee, A. Ledbetter, and L. J. Guo, "Photonic color filters integrated with organic solar cells for energy harvesting," ACS Nano **5**(9), 7055–7060 (2011).
4. Z. Yang, Y. Zhou, Y. Chen, Y. Wang, P. Dai, Z. Zhang, and H. Duan, "Reflective color filters and monolithic color printing based on asymmetric Fabry–Perot cavities using nickel as a broadband absorber," Adv. Opt. Mater **4**(8), 1196–1202 (2016).
5. Z. Yang, Y. Chen, Y. Zhou, Y. Wang, P. Dai, X. Zhu, and H. Duan, "Microscopic interference full-color printing using grayscale-patterned Fabry–Perot resonance cavities," Adv. Opt. Mater. **5**(10), 1700029 (2017).
6. T. Xu, H. Shi, Y. K. Wu, A. F. Kaplan, J. G. Ok, and L. J. Guo, "Structural colors: from plasmonic to carbon nanostructures," Small **7**(22), 3128–3136 (2011).
7. D. P. Langley, E. Balaur, Y. Hwang, C. Sadatnajafi, and B. Abbey, "Optical chemical barcoding based on polarization controlled plasmonic nanopixels," Adv. Funct. Mater. **28**(4), 1704842 (2018).
8. V. R. Shrestha, S. S. Lee, E. S. Kim, and D. Y. Choi, "Aluminum plasmonics based highly transmissive polarization-independent subtractive color filters exploiting a nanopatch array," Nano Lett. **14**(11), 6672–6678 (2014).
9. S. Yokogawa, S. P. Burgos, and H. A. Atwater, "Plasmonic color filters for CMOS image sensor applications," Nano Lett. **12**(8), 4349–4354 (2012).
10. K. T. Lee, S. Seo, J. Y. Lee, and L. J. Guo, "Strong resonance effect in a lossy medium-based optical cavity for angle robust spectrum filters," Adv. Mater. **26**(36), 6324-6328 (2014).
11. K. Seo, M. Wober, P. Steinvurzel, E. Schonbrun, Y. Dan, T. Ellenbogen, and K. B. Crozier, "Multicolored vertical silicon nanowires," Nano Lett. **11**(4), 1851–1856 (2011).

#328166 https://doi.org/10.1364/OE.26.018320
Journal © 2018 Received 13 Apr 2018; revised 7 Jun 2018; accepted 27 Jun 2018; published 2 Jul 2018

Optics EXPRESS

12. J. B. Pendry, D. Schurig, and D. R. Smith, "Controlling electromagnetic fields," Science **312**(5781), 1780–1782 (2006).
13. M. Khorasaninejad, W. T. Chen, R. C. Devlin, J. Oh, A. Y. Zhu, and F. Capasso, "Metalenses at visible wavelengths: Diffraction-limited focusing and subwavelength resolution imaging," Science **352**(6290), 1190–1194 (2016).
14. M. Khorasaninejad, A. Y. Zhu, C. Roques-Carmes, W. T. Chen, J. Oh, I. Mishra, R. C. Devlin, and F. Capasso, "Polarization-insensitive metalenses at visible wavelengths," Nano Lett. **16**(11), 7229–7234 (2016).
15. A. Arbabi, Y. Horie, M. Bagheri, and A. Faraon, "Dielectric metasurfaces for complete control of phase and polarization with subwavelength spatial resolution and high transmission," Nat. Nanotechnol. **10**(11), 937–943 (2015).
16. Z. Li, I. Kim, L. Zhang, M. Q. Mehmood, M. S. Anwar, M. Saleem, D. Lee, K. T. Nam, S. Zhang, B. Luk'yanchuk, Y. Wang, G. Zheng, J. Rho, and C. W. Qiu, "Dielectric meta-holograms enabled with dual magnetic resonances in visible light," ACS Nano **11**(9), 9382–9389 (2017).
17. W. Yue, S. Gao, S. S. Lee, E. S. Kim, and D. Y. Choi, "Highly reflective subtractive color filters capitalizing on a silicon metasurface integrated with nanostructured aluminum mirrors," Laser Photonics Rev. **11**(3), 1600285 (2017).
18. C. S. Park, V. R. Shrestha, W. Yue, S. Gao, S. S. Lee, E. S. Kim, and D. Y. Choi, "Structural color filters enabled by a dielectric metasurface incorporating hydrogenated amorphous silicon nanodisks," Sci. Rep. **7**(1), 2556 (2017).
19. I. Staude, A. E. Miroshnichenko, M. Decker, N. T. Fofang, S. Liu, E. Gonzales, J. Dominguez, T. S. Luk, D. N. Neshev, I. Brener, and Y. Kivshar, "Tailoring directional scattering through magnetic and electric resonances in subwavelength silicon nanodisks," ACS Nano **7**(9), 7824–7832 (2013).
20. M. Decker, I. Staude, M. Falkner, J. Dominguez, D. N. Neshev, I. Brener, T. Pertsch, and Y. S. Kivshar, "High-efficiency dielectric Huygens' surfaces," Adv. Opt. Mater. **3**(6), 813-820 (2015).
21. D. Sell, J. Yang, S. Doshay, K. Zhang, and J. A. Fan, "Visible light metasurfaces based on single-crystal silicon," ACS Photonics **3**(10), 1919–1925 (2016).
22. A. I. Kuznetsov, A. E. Miroshnichenko, M. L. Brongersma, Y. S. Kivshar, and B. Luk'yanchuk, "Optically resonant dielectric nanostructures," Science **354**(6314), 2472 (2016).
23. R. C. Devlin, M. Khorasaninejad, W. T. Chen, J. Oh, and F. Capasso, "Broadband high-efficiency dielectric metasurfaces for the visible spectrum," Proc. Natl. Acad. Sci. U.S.A. **113**(38), 10473–10478 (2016).
24. P. Gutruf, C. Zou, W. Withayachumnankul, M. Bhaskaran, S. Sriram, and C. Fumeaux, "Mechanically tunable dielectric resonator metasurfaces at visible frequencies," ACS Nano **10**(1), 133–141 (2016).
25. S. Sun, Z. Zhou, C. Zhang, Y. Gao, Z. Duan, S. Xiao, and Q. Song, "All-dielectric full-color printing with TiO2 metasurfaces," ACS Nano **11**(5), 4445–4452 (2017).
26. M. S. Sander, M. J. Cote, W. Gu, B. M. Kile, and C. P. Tripp, "Template-assisted fabrication of dense, aligned arrays of titania nanotubes with well-controlled dimensions on substrates," Adv. Mater. **16**(22), 2052-2057 (2004).
27. J. S. King, E. Graugnard, and C. J. Summers, "TiO2 inverse opals fabricated using low-temperature atomic layer deposition," Adv. Mater. **17**(8), 1010-1013 (2005).
28. B. Yang, W. Liu, Z. Li, H. Cheng, S. Chen, and J. Tian, "Polarization-sensitive structural colors with hue-and-saturation tuning based on all-dielectric nanopixels," Adv. Opt. Mater. **6**(4), 1701009 (2018).
29. M. Kerker, D. S. Wang, and C. L. Giles, "Electromagnetic scattering by magnetic spheres," J. Opt. Soc. Am. **73**(6), 765–767 (1983).
30. A. Garcia-Etxarri, "Optical polarization mobius strips on all-dielectric optical scatterers," ACS Photonics **4**(5), 1159–1164 (2017).
31. J. van de Groep and A. Polman, "Designing dielectric resonators on substrates: combining magnetic and electric resonances," Opt. Express **21**(22), 26285–26302 (2013).
32. S. Kruk and Y. Kivshar, "Functional meta-optics and nanophotonics governed by mie resonances," ACS Photonics **4**(11), 2638–2649 (2011).
33. Y. H. Fu, A. I. Kuznetsov, A. E. Miroshnichenko, Y. F. Yu, and B. Luk'yanchuk, "Directional visible light scattering by silicon nanoparticles," Nat. Commun. **4**(1527), 1527 (2013).
34. Lumerical Solutions Inc, "FDTD Solutions," https://www.lumerical.com/tcad-products/fdtd/.

1. Introduction

Color filters have been extensively exploited for a variety of applications, encompassing color imaging and display, organic light-emitting diode devices, solar-cells, color printing, plastic consumer products, anti-counterfeiting, and biosensors [1–10]. Inspired by nature, as in the case of wings of the butterfly, high-performance nano-structural colors can be produced in artificially devised structures from light scattering, diffraction, absorption, or interference [1–6]. Structural color filters are perceived as a prominent alternative to pigment/dye-based materials, which are susceptible to high loss, environmental hazards, difficulty in scalability, performance degradation caused by ultraviolet irradiation and high temperature and

incompatibility with the complementary metal-oxide-semiconductor (CMOS) fabrication process [1–11].

Recently, nanostructured metasurfaces, which refer to an array of ultrathin planar subwavelength elements, have been intensively explored to serve as an alternative platform to conventional diffractive optical elements, rendering the tailoring of amplitude, phase, and polarization of light [12–15]. Diverse nanoscale devices such as color holograms, lenses, and color filters were suggested in metal and/or dielectrics [15–18]. It is observed that plasmonic devices are subject to intrinsic losses in the visible band, which adversely affect their transmission in terms of the spectral shape, bandwidth, and efficiency, resulting in low color gamut and purity. Their scalability is also critically limited [6–10]. Although Fabry-Perot based color filters have been suggested for improving the color gamut and purity [4,5], they suffer lower output efficiency and require the multiple material to form different layer which make the fabrication complicated and costly. High-index nano-resonators that are made up of dielectric materials like silicon [17–22], which are based on electric dipole (ED) and magnetic dipole (MD) resonances mediated by Mie scattering, have been proposed to suppress material absorption and improve efficiency. However, the window of transparency was confined to the infrared region or longer wavelength region of the visible band. Mie scatters in silicon are supposed to face a daunting challenge in generating a distinctive color impression with higher efficiency, especially for blue and yellow color filters [21]. Although SiO_2 and polymers may provide a far wider transparency windows that span the entire visible bands, they are not suitable for producing high quality structural colors because of their low refractive indices. It is of paramount importance that materials and nanofabrication techniques be newly developed, thereby substantially extending the spectral domain of operation of such dielectric metasurfaces beyond the visible band. Amorphous titanium dioxide (TiO_2) can be a prime candidate as base material, in view of its broad transparency window that stretches beyond the visible band. The high-index TiO_2 material, whose interband transition lies just outside of the visible regime, can afford to readily mediate light–matter interactions [23]. In this context, an array of TiO_2 nanocylinders was built through the conventional lift-off method [24], where a coin-shape structure with a low aspect ratio of ~0.5 was introduced. For the filter, the spectral tuning was barely mechanically performed [24]. Although a reflective color filter was embodied tapping into a complicated shape of trapezoidal TiO_2 [25] by virtue of the lift-off technique, the device fabrication entails relatively long-time and multi-step processes. In an attempt to avoid the aforementioned obstacles, we propose atomic layer deposition (ALD) of amorphous TiO_2 [23] to enable the construction of high-aspect-ratio NPs, so that negligible surface roughness and low optical loss could be obtained in the visible band. Our approach is differentiated from previous techniques [26,27] in which the patterns are mostly transferred by a template (e.g., anodic alumina or inverse opal). Highly sophisticated nanostructures can be reliably reproduced thanks to the conformal coating of ALD upon the resist patterns.

In this work, a highly efficient transmissive color filter has been proposed and realized that capitalizes on an all-dielectric metasurface made of TiO_2 NPs of high aspect ratio. Primary subtractive colors of cyan, magenta, and yellow were successfully demonstrated providing large color gamut and purity. The color tunability of the TiO_2 metasurface exhibiting transmission dips has been thoroughly scrutinized depending on the NP diameter, so as to realize a broad range of color images. By inspecting near-field electric and magnetic profiles in relation to the NP and its scattering cross-sections, it has been confirmed that the mechanism bringing about the transmission dips is closely related to the coexistence of ED and MD resonances. The angular tolerance for the device has been finally explored. The proposed device is anticipated to play a vital role in the implementation of image sensors and optical nanoantennas.

Optics EXPRESS

2. Proposed subtractive color filters capitalizing on an all-dielectric metasurface

Figure 1(a) illustrates the configuration of the proposed color filters that incorporate an all-dielectric metasurface, which is composed of an array of TiO_2 NPs of 400-nm thickness (H_g), formed on a glass substrate. For the NP metasurface, the duty cycle is defined as the ratio of the diameter (D) to the period (Λ), which is set at 0.35, and the aspect ratio (H_g/D) is appropriately chosen to ensure enhanced transmission. Figure 1(a) shows that the polarization direction of the incident light is marked by the electric (E) field, which is parallel to the x-direction is transverse electric (TE) polarization, while the magnetic (H) field is parallel to the y-direction. The transverse magnetic (TM) polarization refers to the E-field aligned parallel to y-axis. The proposed devices are presumed to give rise to transmissive subtractive colors of yellow, magenta, and cyan, which can deliver double light throughput compared with their additive counterpart, generating a strong color signal [8]. The proposed filters were designed with the assistance of a simulation tool based on the finite-difference time-domain (FDTD) method (FDTD Solutions, Lumerical Inc., Canada). The dielectric NPs with a high aspect ratio were prepared by utilizing ALD of TiO_2 at a low temperature of 130 °C, thereby avoiding the deformation of resist patterns. The refractive index of the material was measured by ellipsometry (JA Woollam M2000D). Figure 1(b) shows the fabrication procedure adopted for the device, which is addressed in the methods section.

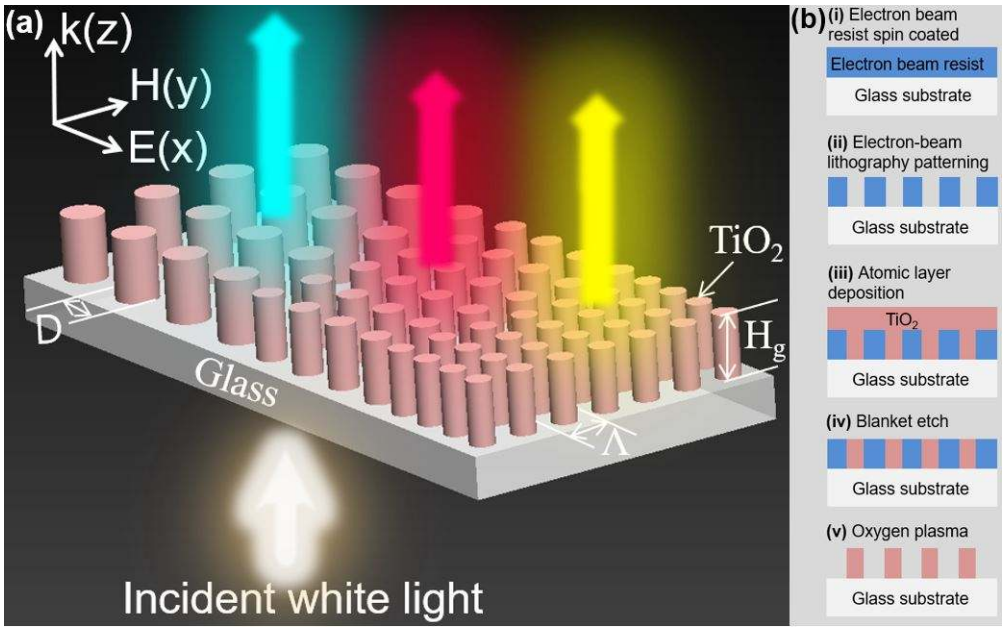

Fig. 1. (a) Schematic of the proposed transmissive color filters based on a metasurface incorporating TiO2 nanopillars, where cyan, magenta, and yellow colors are filtered when white light is incident on the device. (b) Nanofabrication steps for creating the device.

Figure 2(a) shows the scanning electron microscope (SEM) images of the manufactured devices corresponding to primary subtractive colors. Each color filter, with a footprint of 40 µm × 40 µm, produces distinct and vivid colors of yellow, magenta, and cyan, as illustrated in the inset of micrographs for diameters of D = (140, 175, and 210) nm, respectively. A couple of dark spots are witnessed in the images, which stem from fabrication defects such as fallen NPs, and in the case of the yellow filter, they are pronounced. Figure 2(b) shows that the NPs give the highest aspect ratio of about 3. The tilt view (52°) SEM images correspond to the three primary color filters, while the inset for the case of the magenta filter shows the cross-

Optics EXPRESS

sectional SEM image after focused gallium ion beam (FIB) milling. On the whole, the created devices give birth to decent correlations with the design specifications, while minimal surface roughness for the vertical profile is noticed for the TiO_2 NPs. Figure 3(a) shows the simulated and measured transmission spectra for the primary color filters. It was observed that the transmission spectra exhibit double suppressions at the resonance wavelengths for the subtractive colors of yellow, magenta, and cyan. The filter devices delivered high off-resonance transmissions that surpassed 90% in the spectral regime longer than the resonance wavelengths. Figure 3(b) depicts the standard International Commission on Illumination (CIE) 1931 chromaticity diagram, which is commonly used for color evaluation. In the cases of yellow, magenta, and cyan, the simulation and measurement results were in reasonable agreement.

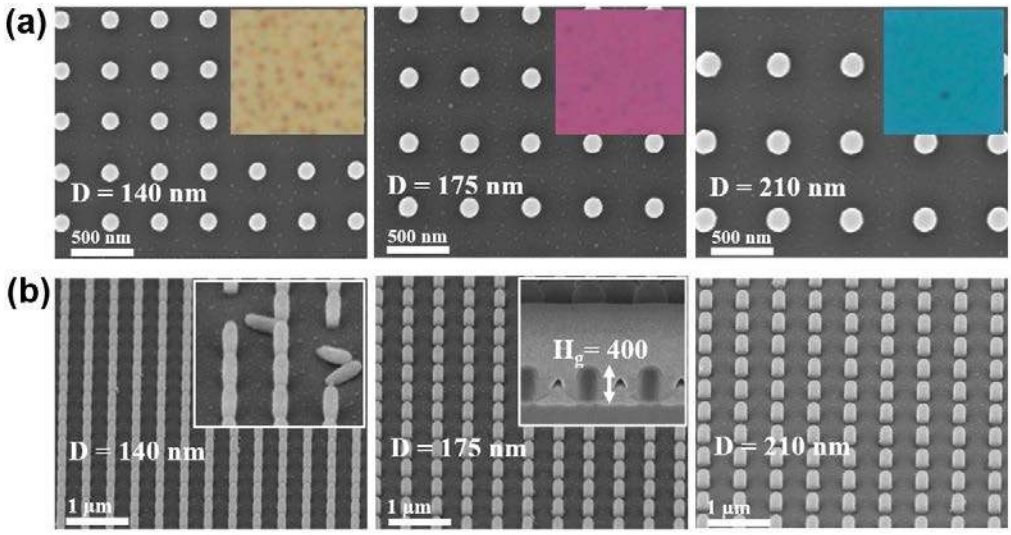

Fig. 2. SEM pictures for the (a) top view and (b) angle view (52°) of the fabricated filters with a footprint of (40 µm x 40 µm) producing vivid yellow, magenta, and cyan color images as shown in the insets for D = (140, 175, and 210) nm, respectively. Some of the fallen NPs are revealed for the yellow case. A FIB image revealing the height of the fabricated NPs is included in the inset of angle view for the magenta filter.

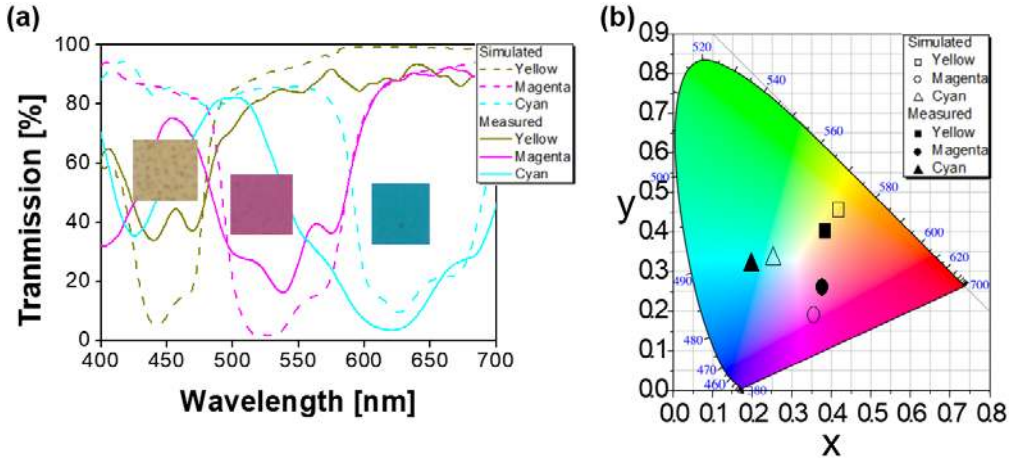

Fig. 3. (a) Simulated and measured transmission spectra for the three primary subtractive colors of yellow, magenta, and cyan. (b) Corresponding CIE 1931 chromaticity color response for both the simulated and measured spectra.

Optics EXPRESS

Figure 4(a) shows the evolution of the resonance wavelengths relating to the dips in the transmission spectra for the TiO_2 metasurface for the (i) simulated and (ii) measured cases when the NP diameter varies from (126 to 224) nm in steps of 7 nm. The pattern signifies the influence of the NP diameter on the color tuning. The black dashed (for the ED) and the blue dashed (for the MD) lines, traces the resonant dip positions, apparently overlap for the simulated and measured spectra. The inset in Fig. 4(a) (ii) presents the color images for the fabricated filters with different diameter and Fig. 4(b) displays the corresponding CIE 1931 chromaticity diagram for (i) the simulated and (ii) the measured cases. The transmission spectra with broader bandwidth in the subtractive mode, as depicted in Fig. 4(a), is desired to produce the vivid colors response as plotted in CIE 1931 chromaticity diagram shown in the Fig. 4(b). The disparities between the simulated and measured spectra are principally ascribed to the fabrication inaccuracies, including deviations from the perfect cylindrical shape of TiO_2 NPs, in conjunction with surface and sidewall roughness. The sidewall roughness of TiO_2 pillars is determined by that of ZEP520 resist holes, which is known to be 1-2 nm RMS roughness. Also, the pillar top roughness, resulting from the TiO_2 deposition and shallow blanket etching (~20 nm etch depth), has a similar range of roughness. Therefore, the effect of roughness on the optical performance of the filters might be marginal. We measured the dispersion of TiO_2, film deposited based on ALD technique, as shown in appendix A. The extinction coefficient was below 0.001 in the visible spectrum, indicating a negligible absorption loss from 400-nm-thick TiO_2 film. The deviation from the perfect cylindrical shape to other shapes like ellipsoidal pillars might result in the different spectral shape and hence the color saturation. It is stated that the saturation of the subtractive colors is dependent on the bandwidth, near-zero resonant dip in conjunction with a high off-resonance transmission efficiency [8]. It has been reported that the bandwidth is controlled to generate different colors and improve saturation of the colors using an ellipsoidal pillar [28].

Optics EXPRESS

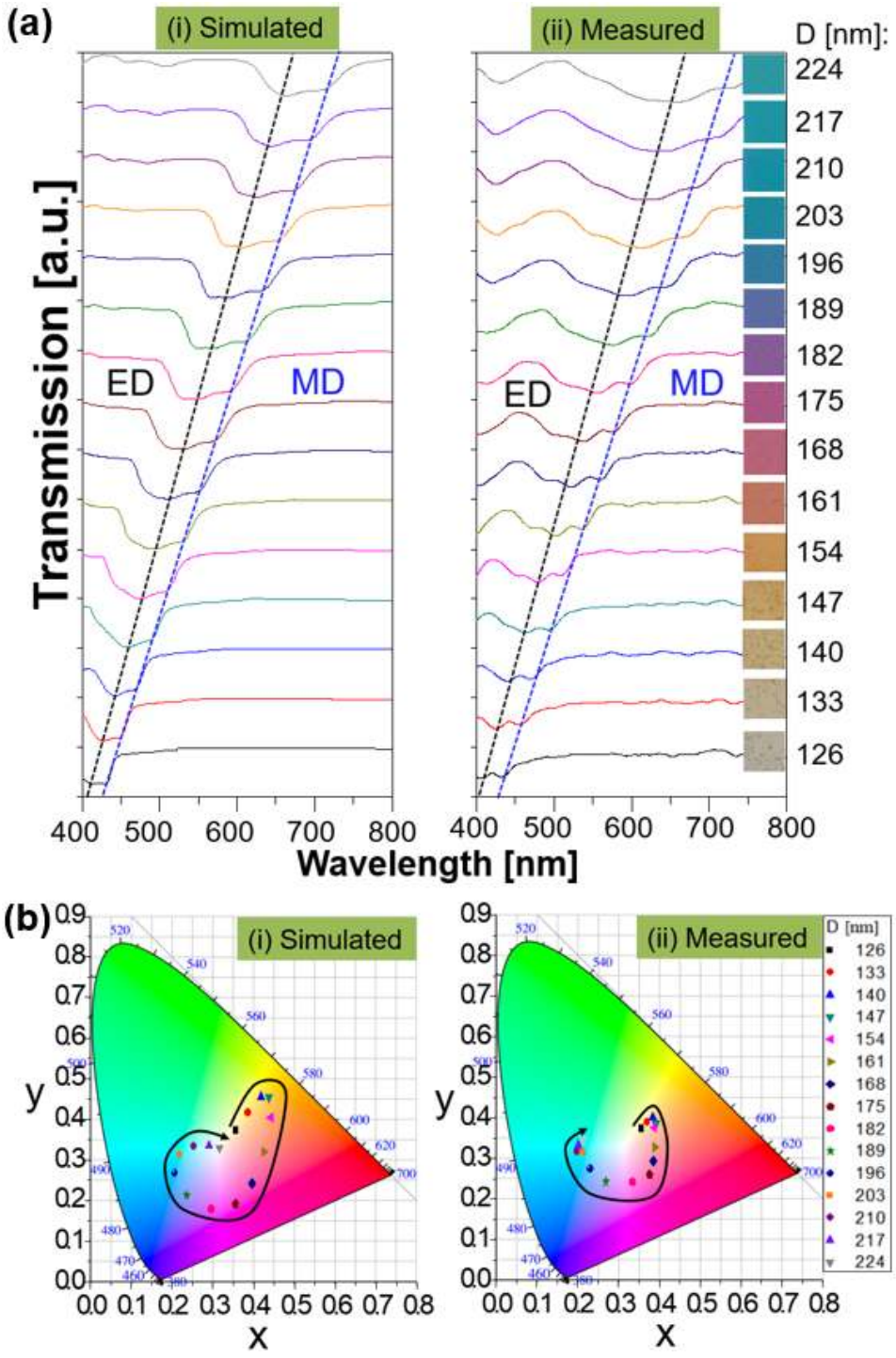

Fig. 4. (a) (i) Simulated and (ii) measured transmission spectra for the color filter with D = (126 to 224) nm in steps of 7 nm. The resonant transmission dips correspond to the ED and MD modes that are traced by black and blue dashed lines, respectively. Inset of (ii) shows the captured vivid color images for the devices of concern. (b) CIE 1931 chromaticity color response for the (i) simulated and (ii) measured transmission spectra.

Optics EXPRESS

3. Mechanism underlying the transmission dips for the metasurface based on TiO_2 NPs

For a metasurface comprised of an array of TiO_2 NPs, each NP element is perceived to act as a resonator, allowing for the excitation of ED and MD modes by virtue of the Mie scattering [17–20]. Each NP is equivalent to a dielectric waveguide that is truncated on both ends, serving as a low-quality factor Fabry-Perot etalon. The effective refractive indices of the NP resonator are keenly dependent on its diameter [15]. In an effort to discover the key mechanism underpinning the spectral transmission dips, the NP has been rigorously checked in terms of the E- and H-field profiles at resonance in combination with the scattering cross-section. Figure 5(a) (i) depicts the spectral transmission that exhibit dips centered at the wavelengths of (530 and 560) nm, for a typical filter with D = 175 nm. Figure 5(a) (ii) shows the calculated scattering cross-section for the NP, where the cross-section peaks are concurrent with the resonance dips, supporting the thesis that the scattering mostly dictates the spectral transmission. Figures 5(b) and 5(c) present the field profiles in relation to the resonant ED and MD modes initiated by the scattering, respectively. In particular, Figs. 5(b) (i) and 5(c) (i) show the respective E- and H-field profiles in the xy plane at the height of 300 nm above the TiO_2-glass interface. The ED mode, monitored at the wavelength of 530 nm, is signified by the reinforced E-field as shown in Fig. 5(b) (ii) in combination with the current loop for the H-field shown in the vector plot in Fig. 5(b) (iii), on the yz cross-section that cuts through the center of the TiO_2 NP. While the MD mode at 560 nm wavelength is proclaimed by the circular displacement current associated with the E-field, which is shown in the vector plot in Fig. 5(c) (ii), in combination with the reinforced H-field shown in Fig. 5(c) (iii) on the xz cross-section that cuts through the center of the TiO_2 NP. The black dashed line stands for the interface between two different media. The presence of the neighboring ED and MD modes is responsible for the spectral resonance broadening [19,31]. The ED and MD excitations can be better distinguished under different aspect ratios and duty ratios [16,17]. A strong MD is deemed to be induced when the wavelength within the nanostructure becomes comparable to its dimension, under the condition of $2R \approx \lambda/n$, where n is the refractive index, R the radius, and λ the wavelength. A subwavelength nanoparticle ($R < \lambda$) requires a large index of refraction and thus facilitates such resonance [32]. Simultaneous occurrence of the ED and MD has been attributed to the Kerker's-type scattering [29,30,33].

Optics EXPRESS

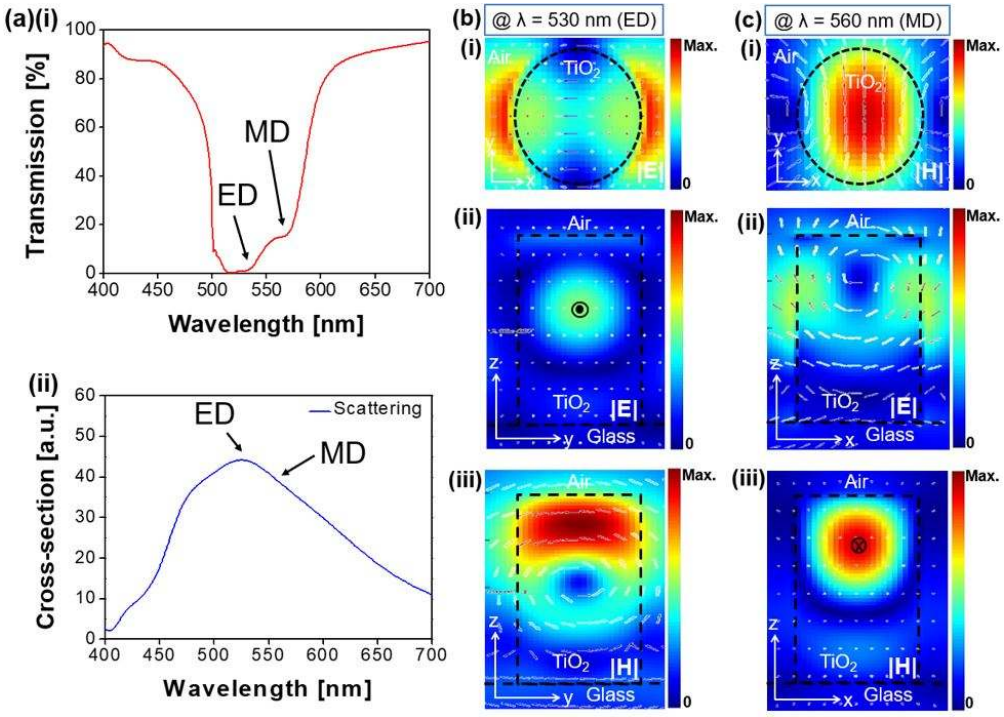

Fig. 5. (a) (i) Simulated transmission spectra with resonant dips and (ii) Calculated scattering cross-sections. The positions of ED and MD on the spectrum are pointed with arrows. The cross-section associated with the electric and magnetic field profiles for the (b) ED resonance at λ = 530 nm and (c) MD resonance at λ = 560 nm, for the color filter with D = 175 nm.

The proposed color filter drawing upon an all-dielectric metasurface is notable for its capability to attain affordable angular tolerance, as shown in Figs. 6(a) and 6(b), for TE and TM polarizations, respectively. The transmission dips and the maximum off-resonance transmission greater than 90% are observed to be maintained up to an incidence angle of 10°, for both polarizations. The observed relaxed angular tolerance makes the proposed filters suitable for their potential implementation in the color displays, imaging, and color printing. The transmission spectra were also scrutinized with respect to the TiO_2 height, for both polarizations, as shown in Fig. 6(c). The height of the TiO_2 NP was fixed at 400 nm, which guarantees an appropriate spectral response and decent coloration throughout the visible band, with the height ranging from (100 to 500) nm.

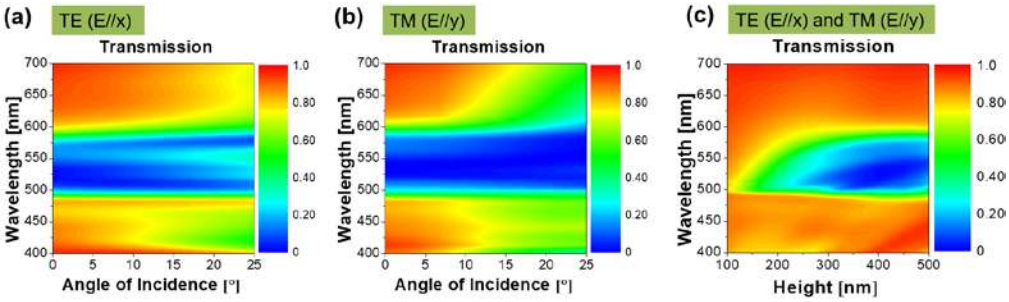

Fig. 6. Calculated transmission spectra for (a) angular performance for TE polarization, (b) angular performance for TM polarization, and (c) effect of height for both TE and TM polarizations, for a typical filter with the D = 175 nm.

Optics EXPRESS

4. Methods

4.1 Device fabrication

The cell constituting the proposed color filter was designed and created to exhibit dimensions of 40 µm × 40 µm. For the fabrication of the TiO_2 metasurface, a 400-nm-thick electron-beam resist (ZEP 520A from Zeon, Japan) was spin-coated on a glass substrate; then, electron-beam lithography (Raith150) was applied to make a pattern of circular holes. The distortion of pattern dimension and shape due to the proximity effect was minimized by applying high electron beam energy (30kV) and the small duty ratio of the holes. ALD was used to conformally deposit TiO_2 on the developed holes, where the deposition rate was around 60 nm per hour. We applied around two hours' deposition for complete filling of the largest nanopillars (D = 210 nm). Subsequently, a TiO_2 blanket etch was performed using CHF_3 plasma to reach up to the resist surface. Finally, the electron-beam resist was removed by oxygen plasma.

4.2 Optical characterization

The fabricated TiO_2 pattern was visually inspected by dual beam (SEM/FIB) high-resolution scanning electron microscopy (FIB II, Quanta 3D FEG, FEI). The transmission spectra were checked by launching a collimated beam from a halogen lamp (HL-2000-FHSA, Ocean Optics), which was polarized through a calcite crystal polarizer (GTH 10M-A, Thorlabs), to the prepared color filter mounted on a motorized rotation stage. The optical output was captured by spectrometry (Avaspec-3648, Avantes) via a multimode fiber. Images for each color were taken via digital microscopy (Leica DM4000 M).

4.3 Numerical simulations

The transmission/reflection spectra, scattering cross-sections, and field profiles for the proposed devices were investigated by means of a simulation tool based on the finite difference time domain (FDTD) method (FDTD Solutions, Lumerical Inc., Canada) [34]. A normally incident plane wave was illuminated to a unit cell that satisfies a periodic boundary condition, thereby mimicking an array of TiO_2 NPs. The dispersion characteristics of TiO_2 in the visible spectral range, which were observed through an ellipsometer (JA Woollam M2000D), were reflected in the simulations, and the dispersion characteristics of SiO_2, which are used for the simulations were derived from the multi-coefficient model supplied by the simulation tool [34].

5. Conclusion

We realized highly efficient transmissive-type color filters that utilize an all-dielectric metasurface that incorporates high aspect ratio of TiO_2 NPs on a glass substrate. Primary subtractive colors of cyan, magenta, and yellow were demonstrated that exhibited large color gamut and purity. A suite of filter devices with different NP diameter was manufactured to demonstrate the broad range of color tuning in the visible band. The prepared color filters provide a transmission efficiency beyond 90%, enabling high resolution and excellent color fidelity. The transmission dips are supported by the simultaneous excitation of the ED and MD modes, which are well depicted with the help of the near-field profiles of E-field and H-field. The dips in the transmission spectra and the position of the peaks in the calculated scattering cross-sections correlate with each other. The proposed color filter will make it an outstanding candidate for implementing various applications that include high-performance optical nanoantennas, beam-steering, beam-shaping devices, and so forth.

Funding

National Research Foundation of Korea (NRF), funded by the Korean government (MSIP) (No. 2016R1A2B2010170); Kwangwoon University; Australian Research Council Future Fellowship (FT110100853, Dr. Duk-Yong Choi).

Acknowledgements

The authors are grateful to Mr. Chul-Soon Park and Mr. Song Gao for their valuable help. This work was performed in part at the ACT node of the Australian National Fabrication Facility.

Appendix A: Dispersion characteristics of TiO_2

Figure 7 shows the refractive index vs wavelength of TiO_2 in the visible band used for the simulation. The dispersion characteristics of the TiO_2 were measured by ellipsometry (JA Woollam M2000D) in the visible spectral range and were reflected in the simulations. The ALD was used for the deposition of TiO_2 at the relatively low temperature of ~130 °C.

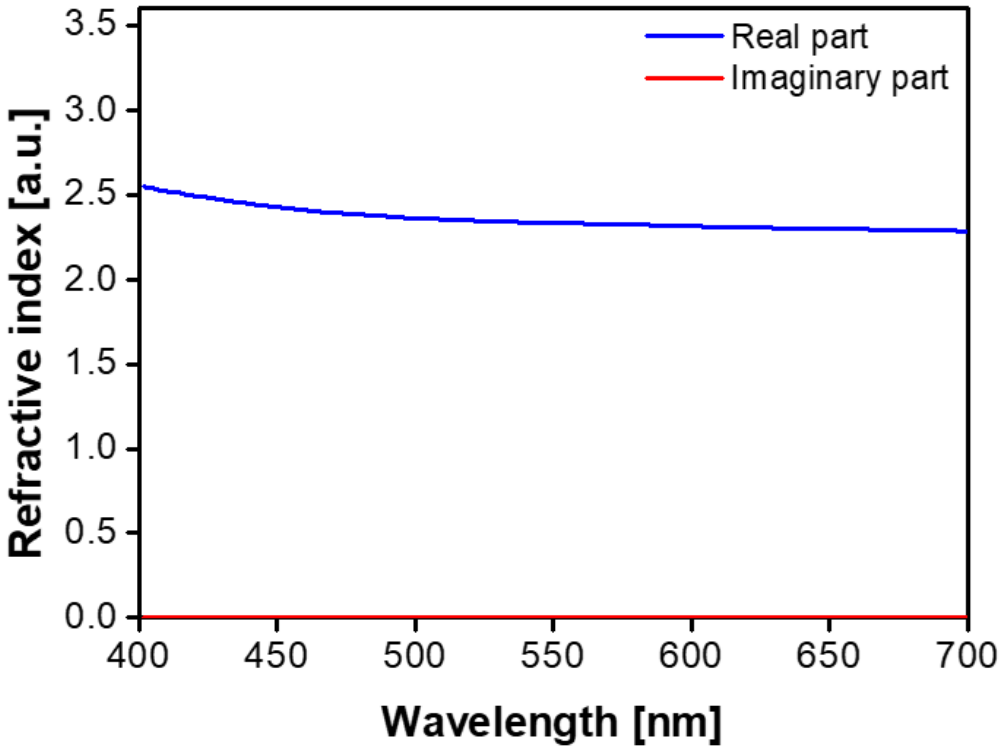

Fig. 7. Dispersion characteristics of the TiO_2 deposited by atomic layer deposition (ALD) technique.